Mon. Not. R. Astron. Soc. **000**, 1–14 (2002)   Printed 25 August 2015   (MN LaTeX style file v2.2)

arXiv:1507.04175v3 [astro-ph.SR] 24 Aug 2015

The WISE View of RV Tauri Stars

I. Gezer[1,2], H. Van Winckel[2], Z. Bozkurt[1], K. De Smedt[2], D. Kamath[2],
M. Hillen[2] and R. Manick[2]
[1]*Astronomy and Space Science Department, Ege University ,35100 Bornova, Izmir, Turkey*
[2]*Institute of Astronomy, KU Leuven, Celestijnenlaan, 200D 3001 Leuven, Belgium*

25 August 2015

ABSTRACT

We present a detailed study based on infrared photometry of all Galactic RV Tauri stars from the General Catalogue of Variable Stars (GCVS). RV Tauri stars are the brightest among the population II Cepheids. They are thought to evolve away from the asymptotic giant branch (AGB) towards the white dwarf domain. IRAS detected several RV Tauri stars because of their large IR excesses and it was found that they occupy a specific region in the [12] − [25], [25] − [60] IRAS two-colour diagram. We used the all sky survey of WISE to extend these studies and compare the infrared properties of all RV Tauri stars in the GCVS with a selected sample of post-AGB objects with the goal to place the RV Tauri pulsators in the context of post-AGB evolution. Moreover, we correlated the IR properties of both the RV Tauri stars and the comparison sample with other observables like binarity and the presence of a photospheric chemical anomaly called depletion. We find that Galactic RV Tauri stars display a range of infrared properties and we differentiate between disc sources, objects with no IR excess and objects for which the spectral energy distribution (SED) is uncertain. We obtain a clear correlation between disc sources and binarity. RV Tauri stars with a variable mean magnitude are exclusively found among the disc sources. We also find evidence for disc evolution among the binaries. Furthermore our studies show that the presence of a disc seems to be a necessary but not sufficient condition for the depletion process to become efficient.

Key words: circumstellar matter – infrared: stars –stars: variables: Cepheids – stars: AGB and Post-AGB.

1 INTRODUCTION

RV Tauri stars are luminous population II Cepheid variables with spectral types typically between F and K. They are named after the prototype RV Tau. According to the GCVS (Samus et al. 2009), there are 153 RV Tauri variables in our Galaxy and several have been found in the LMC and SMC (Alcock et al. 1998; Soszyński et al. 2008; Buchler et al. 2009; Soszyñski et al. 2010). In this paper, we focus on the Galactic sample.

Characteristic and defining light curves of RV Tauri stars show subsequent deep and shallow minima (e.g. Pollard et al. 1997). Their formal pulsation period is in between 30 and 150 days and the amplitude may reach up to 4 magnitudes in V. The pulsations of RV Tauri stars can be regular, however, irregular pulsations are more commonly detected. There are several explanations for the light variations (Tuchman et al. 1993). Non-linear, non-adiabatic hydrodynamical RV Tauri models (Fokin 1994) support the hypothesis in which a resonance between the fundamental mode and the first overtone is responsible for the alternating minima in the light curves.

RV Tauri stars are divided into two photometric subclasses based on the characteristics of the light curve (Kukarkin 1958). These subclasses are indicated with letter **a** and **b**. The RVa stars have a constant mean magnitude, while the RVb stars have a varying mean magnitude on a time scale between 600 and 1500 days (Samus et al. 2009). In addition to the photometric subclasses, RV Tauri stars are divided into three spectroscopic subclasses (Preston et al. 1963). These subclasses are labelled as **A**, **B**, **C**. The stars of type RVA are of spectral type G-K, and show strong absorption lines and normal CN or CH bands while TiO bands sometimes appear at photometric minimum. RVB stars are generally somewhat hotter, weaker lined objects which show enhanced CN and CH bands. RVC stars are also weak lined but they show normal bands of CH and CN. This last subclass contains the globular cluster members of the RV Tauri class. There is no correlation between the spectroscopic and photometric classes.

Earlier pioneering ground-based detections of IR excesses in some RV Tauri stars (AC Her, U Mon, R Sct, R Sge) (Gehrz & Woolf 1970; Gehrz & Ney 1972; Gehrz 1972) were followed by systematic full-sky surveys once IR satellites were launched. A limited number of RV Tauri stars were detected by IRAS (Infrared Astronomical Satellite 1983) confirming the ground-based detections of some, and enlarging the sample for which a large IR excess due to the thermal emission from circumstellar dust was found. This was used to classify RV Tauri stars as post-Asymptotic Giant Branch (post-AGB) stars by Jura (1986). Assuming that the RV Tauri stars are pulsating post-AGB stars which are crossing the instability strip, one may expect that the photospheres are enriched by AGB nucleosynthesis products. Indeed, a rich nucleosynthesis occurs on the AGB evolutionary phase, where carbon, nitrogen, and the slow neutron capture (*s*-process) elements beyond iron are produced. Recurrent mixing episodes, induced by the thermal pulses on the AGB transport the freshly synthesized material to the surface (e.g. Herwig 2005). Therefore, abundances of Galactic RV Tauri stars have been extensively studied over the past two decades. These studies show that RV Tauri stars are mainly *not* enriched in C and s-process elements (e.g. Giridhar et al. 1994, 1998, 2000; Gonzalez et al. 1997a,b; Van Winckel et al. 1998; Maas et al. 2002, 2003, 2005; Deroo et al. 2005). Earlier work suggested, for instance, the two prototypical RV Tauri stars AC Her and RU Cen to be C-enriched, based on their high [C/Fe] (Gehrz & Woolf 1970; Gehrz & Ney 1972). Also the dust component in these two objects was presumed to be C-rich. Both assertions are, however, no longer supported by more recent works, like the photospheric abundance analysis of Van Winckel et al. (1998) and the dust studies of Molster et al. (2002), Molster et al. (2002), Molster et al. (2002), Gielen et al. (2007, 2009); Hillen et al. (2015). One exception may be V453 Oph, which shows a mild *s*-process overabundance but it is not accompanied by C enhancement (Deroo et al. 2005). Also the abundance analysis results on a LMC sample of RV Tauri stars (Reyniers et al. 2007; Reyniers & Van Winckel 2007) showed that C and *s*-process enrichments are generally not found with one exception being MACHO 47.2496.8 which shows a strongly enriched photosphere (Reyniers et al. 2007).

While C and *s*-process enrichments are generally not found, many RV Tauri photospheres show a distinct chemical anomaly which is called "depletion". Depleted photospheres display a similar chemical composition as the gas phase of the interstellar medium: refractory elements, which have high dust condensation temperature, are underabundant, while volatiles, which have low condensation temperature, are more abundant (e.g. Van Winckel 2003). The process to acquire the chemical anomaly is not completely understood yet, but it must be a chemical rather than a nucleosynthetic process. Dust formation may lead to a chemical fractionation event in the circumstellar environment. To obtain a depleted photosphere, the radiation pressure on circumstellar dust grains must fractionate the dust from the gas. The cleaned gas is then re-accreted onto the stellar surface. As a result of this process, stars display peculiar photospheric composition similar to the interstellar gas.

The recurrent chemical anomalies found in RV Tauri stars make that the evolutionary nature of these pulsators are still not clear. In this contribution we focus on the dust excesses. Lloyd Evans (1985) showed that infrared colours of RV Tauri stars occupy a specific region in the IRAS [12]-[25], [25]-[60] diagram (see Fig. 1) and he defined this region as the *RV Tauri Box*. Unfortunately, IRAS colours are available for only 18 RV Tauri stars.

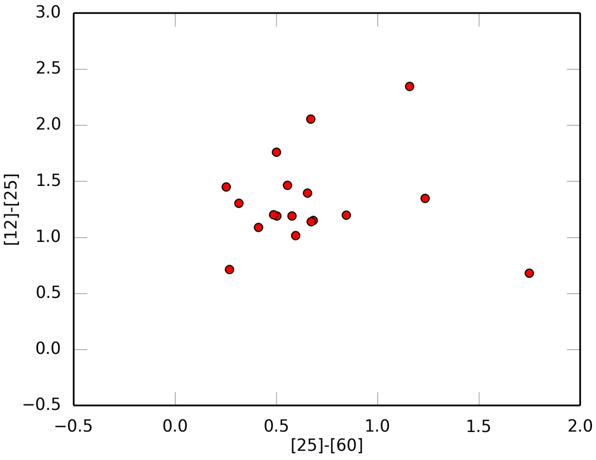

Figure 1. IRAS colour-colour diagram for RV Tauri stars, RV Tau box (Lloyd Evans 1985).

Here, we present a systematic study of the IR properties of RV Tauri stars and we use all Galactic RV Tauri stars listed in the GCVS (Samus et al. 2009) as our sample. The IR photometry is a good tracer of the temperature gradient of the circumstellar dust (if present), which we want to correlate with the properties of the central object. We expand the RV Tauri study based on IRAS colours to a similar but much deeper one using WISE (Wide-field Infrared Survey Explorer) data. The WISE satellite was launched in December 2009 and scanned the whole sky in 3.4, 4.6, 12 and 22 μm bands (Wright et al. 2010). The biggest advantage is that the WISE survey is deep enough to detect all Galactic RV Tauri stars of our sample.

The WISE photometric bands are not the same as the IRAS bands, so we defined a new colour combination [3.4]−[4.6] (W1-W2) versus [12]−[22] (W3-W4) as a good WISE alternative, be it more focussed on the near- and mid-IR. The [3.4]−[4.6] colour is a good indicator for the presence of a near IR excess while the [12]−[22] colour is indicative of the presence of cooler dust. In order to compare the Galactic RV Tauri stars with post-AGB objects, we compose a reference sample, which consist of 60 well-known dusty optically bright post-AGB stars.

Our samples and the WISE colour-colour diagram are presented in Sect. 2. In Section 3 we study the correlation between the colours and other observational properties of RV Tauri stars and compare the RV Tauri sample with the well defined post-AGB stars. The relation between IR excess, binarity and chemical anomalies are discussed in section 4. Conclusions are summarized in Sect. 5.

2 REFERENCE SAMPLE

Since RV Tauri stars are a subset of post-AGB objects we compare the Galactic RV Tauri stars with Galactic post-AGB objects that do not display the RV Tauri light curves.

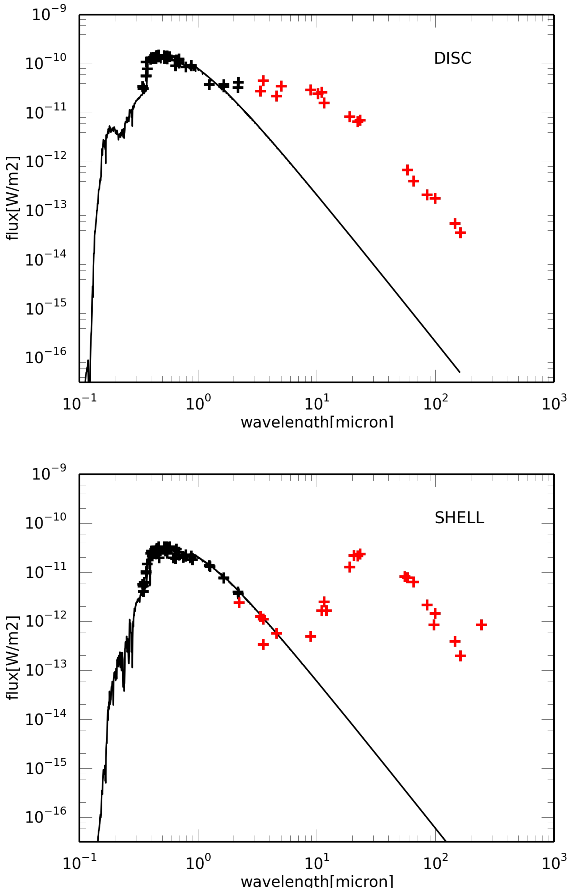

Figure 2. Characteristic SEDs of optically bright post-AGB stars. Top panel: the SED of 89 Her which is a well-known binary system. The solid line represents the photospheric flux of the model atmosphere, the black crosses the dereddened photometric data. The red plusses show the IR photometric data, pointing to the presence of a compact disc (Hillen et al. 2014). The bottom panel shows the SED of HD 161796, the solid line represents the photosphere, the black crosses the dereddened measurements, while the red crosses show the IR data, pointing to the presence of an expanding dusty shell (Min et al. 2013).

To do this we have defined a reference sample of well characterised Galactic post-AGB stars. Optically bright post-AGB stars show typically two different types of SED (see Fig. 2) (Van Winckel 2003). The first group of post-AGB stars display SEDs with a broad IR excess starting in the near-IR region, which points to the presence of hot dust near the star. The [3.4]-[4.6] colour is a good identifier for these sources which are called *disc* sources (see section 2.1). The second group contains post-AGB stars with a double peaked SED (see Fig. 2) where the first peak corresponds to the photospheric flux and the second peak represents the IR emission of an expanding dusty envelope. In the outflow model for a single post-AGB star, the near-infrared excess is expected to disappear within years after the cessation of the dusty mass loss. The mid-infrared excess is an indicator of this detached expanding circumstellar envelope (CSE). The [12]-[22] colour is a good identifier for these sources which are called *shell* sources (see section 2.2).

For 60 carefully selected reference post-AGB objects, we determined the full SEDs from the available photometric data by using the Vizier database (Ochsenbein et al. 2000). Scaled Kurucz models (Castelli & Kurucz 2003) were determined for the given stellar parameters (Teff, logg and [Fe/H]) obtained from the literature and given in Table 1. The total line-of-sight reddening was determined by minimizing the difference between the scaled reddened atmospheric model and the photometric data with the grid-method explained in Degroote et al. (2011). In total we have selected 33 disc and 27 shell sources as reference sample for our study.

2.1 Disc sources

c

In recent years a lot of observational evidence has been accumulated that SEDs which show a near IR-excess are indicative for the presence of a stable compact dusty disc (e.g. de Ruyter et al. 2006; Deroo et al. 2006, 2007; Gielen et al. 2011; Hillen et al. 2015). The dust grain processing both in dust grain growth and crystallinity is very strong, which are indicators for the longevity (e.g. Gielen et al. 2008, 2011) and the IR spectra of disc sources clearly stand out compared to expanding shells. Mid- and near-IR interferometric measurements are needed to resolve the discs and show indeed that the very compact nature of the circumstellar environment (e.g. Deroo et al. 2006; Hillen et al. 2013, 2014). In two objects the Keplerian kinematics has been resolved via CO interferometric data obtained at the Plateau de Bure (Bujarrabal et al. 2015) and ALMA (Bujarrabal et al. 2013) interferometers. Single disc CO observations often show a narrow CO profile, again indicative of Keplerian kinematics rather than expansion (Bujarrabal et al. 2013). Our reference sample contains 33 disc objects with the disc sample mainly build from de Ruyter et al. (2006) and more recent additions (Table 1). WISE photometry has a saturation limit for the very bright sources. Sources brighter than approximately 2.0, 1.5, -3.0 and -4.0 magnitude in W1, W2, W3 and W4 respectively, are not reliable. Therefore, sources for which the WISE photometry suffers from saturation are not represented in the WISE colour-colour diagram but are included in Table 1 for completeness. These objects are HD 44179, which is the central star of the famous Red Rectangle nebula, HR 4049, IRAS 10456−5712 and IRAS 09371+1212 which is known as the Frosty Leonis nebula.

2.2 Shell sources

After the AGB phase, the expansion of the remnant CSE around a single post-AGB star is thought to produce a detached circumstellar shell. These objects are expected to display a double-peaked SED. The expansion velocity of the gas as well as the mass-loss rates can be determined by CO observations (Bujarrabal 1999). A typical expansion velocity for the circumstellar shell is 10 to 15 km/s (Hrivnak et al. 2000; He et al. 2014). We made an extensive literature survey for optically bright objects for which the envelope kinematics are studied using the rotational transition of CO (see Table 1). We selected 27 post-AGB stars which show a clear double peak SED and an CO expansion velocity between 10 and 15 km/s and we characterise them as *shell* sources.

Table 1. Reference sample, consisting of well selected and observationally characterized post-AGB objects.

IRAS	Other Name	RA	DEC	Spectral Type	[12]−[22]	[3.4]−[4.6]	SED	Ref
01427+4633	BD+46 442	01 45 47.03	+46 49 00.97	F2III	1.434	0.83	disc	2
04296+3429		04 32 56.97	+34 36 12.40	G0Ia	2.536	1.055	shell	12,7
05040+4820	BD+48 1220	05 07 50.30	+48 24 09.42	A4Ia	6.095	0.081	shell	7,8
05089+0459		05 11 36.15	+05 03 26.30	M3I	2.511	0.875	shell	7
05113+1347		05 14 07.76	+13 50 28.30	G8Ia	2.908	0.514	shell	7,16
05208−2035		05 22 59.42	−20 32 53.03	Me...	1.293	0.824	disc	1
05238−0626	BD−06 1178	05 26 19.76	−06 23 57.40		2.468	0.291	shell	7
05341+0852		05 36 55.05	+08 54 08.68	F5I	2.225	1.065	shell	12,7
05381+1012	HD 246299	05 40 57.05	+10 14 24.99	G2/G3I	2.671	0.34	shell	7
06160−1701	UY CMa	06 18 16.37	−17 02 34.72	G0V	1.24	1.33	disc	1
06176−1036*	HD 44179	06 19 58.22	−10 38 14.71	B8V	—	—	disc	1
06338+5333	HD 46703	06 37 52.43	+53 31 01.96	F7IVw	0.96	0.271	disc	1
06472−3713	ST Pup	06 48 56.41	−37 16 33.34	G2I	1.625	1.31	disc	1
06530−0213		06 55 31.82	−02 17 28.30	G1I	2.643	0.424	shell	6
07008+1050	HD 52961	07 03 39.63	+10 46 13.06	A0	0.922	0.985	disc	1
07134+1005	HD 56126	07 16 10.26	+09 59 47.99	F5Iab	2.527	0.137	shell	11,12
07140−2321	SAO 173329	07 16 8.27	−23 27 01.61	F5	1.393	1.128	disc	1
07171+1823		07 20 1.53	+18 17 26.12	BQ[]	3.15	0.955	shell	7
07430+1115		07 45 51.39	+11 08 19.60	G5Ia	2.544	0.646	shell	7
08187−1905	HD 70379	08 20 57.10	−19 15 03.47	F6Ib/II	4.551	0.069	shell	6
09060−2807		09 08 10.13	−28 19 10.39	F5	1.067	1.461	disc	1
09371+1212*	Frosty Leo	09 39 53.96	+11 58 52.60	M4	—	—	shell	19
10158−2844*	HR 4049	10 18 7.59	−28 59 31.20	B9.5Ib-II	—	—	disc	1
10174−5704		10 19 16.89	−57 19 26.00	G8IaO	1.672	1.192	disc	1
10456−5712*		10 47 38.40	−57 28 02.68	M1II	—	—	disc	1
11000−6153	HD 95767	11 02 4.31	−62 09 42.84	F2III	0.965	1.689	disc	1
11472−0800		11 49 48.04	−08 17 20.47	F5Iab:	1.798	1.723	disc	1
12222−4652	HD 108015	12 24 53.50	−47 09 07.51	F4Ib/II	1.157	1.797	disc	1
13258−8103		13 31 7.05	−81 18 30.40	F4Ib-G0Ib	2.022	1.272	disc	1
14488−5405		14 52 28.72	−54 17 42.80		3.468	0.791	shell	18
14524−6838	EN TrA	14 57 00.68	−68 50 22.89	F2Ib	1.097	1.592	disc	1
15039−4806	HD 133656	15 07 27.44	−48 17 53.87	A1/A2Ib/II	4.763	0.048	shell	5
15469−5311		15 50 43.80	−53 20 43.33	F3	1.449	1.624	disc	1
15556−5444		15 59 32.57	−54 53 20.40	F8	1.212	1.929	disc	1
16230−3410		16 26 20.39	−34 17 12.76	F8	1.314	1.48	disc	1
17038−4815**		17 07 36.64	−48 19 08.56	G2p...	1.199	1.501	disc	1
17074−1845	BD−18 4436	17 10 24.15	−18 49 00.67	B5Ibe	4.448	0.15	shell	13
17233−4330		17 26 58.65	−43 33 13.47	G0p...	1.423	1.834	disc	1
17243−4348	LR Sco	17 27 53.62	−43 50 46.27	G2	1.231	1.715	disc	1
17436+5003	HD 161796	17 44 55.47	+50 02 39.48	F3Ib	4.418	0.127	shell	10
17534+2603	89 Her	17 55 25.19	+26 02 59.97	F2Ibe	1.106	0.728	disc	1
18095+2704	V887 Her	18 11 30.67	+27 05 15.61	F3Ib	2.322	0.773	shell	17
18123+0511		18 14 49.39	+05 12 55.70	G5	1.471	1.765	disc	1
18158−3445		18 19 13.37	−34 44 30.00	F6	1.59	1.379	disc	1
18379−1707		18 40 48.62	−17 04 38.30	B1IIIpe	4.111	0.672	shell	13
19114+0002	HD 179821	19 13 58.61	+00 07 31.93	G5Ia	3.676	0.629	shell	14
19135+3937		19 15 12.14	+39 42 50.51		1.306	1.214	disc	2
19157−0247		19 18 22.71	−02 42 10.89	B1III	1.221	1.713	disc	1
19410+3733	HD 186438	19 42 52.92	+37 40 41.46	F3Ib	0.915	1.395	disc	4
19475+3119	HD 331319	19 49 29.56	+31 27 16.22	F8	5.242	0.093	shell	9
19500−1709	HD 187885	19 52 52.70	−17 01 50.30	F2/F3Iab+...	2.564	0.367	shell	12,15
19580−3038	V1711 Sgr	20 01 7.98	−30 30 38.89	F5.2:...	1.234	1.167	disc	3
20000+3239		20 01 59.52	+32 47 32.90	G8Ia	2.645	0.955	shell	14
20056+1834	QY Sge	20 07 54.62	+18 42 54.50	G0e...	1.135	2.017	disc	1
22223+4327	V448 Lac	22 24 31.43	+43 43 10.90	F9Ia	4.207	0.274	shell	12,14
22272+5435	HD 235858	22 29 10.37	+54 51 06.35	G5Ia	2.838	1.286	shell	15
22327−1731	HD 213985	22 35 27.53	−17 15 26.89	A0III	1.353	1.182	disc	1
23304+6147		23 32 44.79	+62 03 49.10	G2Ia	2.908	0.432	shell	7,15
Z02229+6208		02 26 41.79	+62 21 22.00		2.546	1.194	shell	6
	BD+39 4926	22 46 11.23	+40 06 26.30	B8	2.046	-0.008	disc	1

∗WISE data indicates saturation.

∗∗Although an RV Tauri pulsator (Lloyd Evans (1999); Kiss et al. (2007), but not in the GCVS) we include this object in the reference sample because it is a well characterized disc object.

(1):de Ruyter et al. (2006); (2):Gorlova et al. (2012); (3):Maas et al. (2007); (4):Oudmaijer et al. (1995); (5):Van Winckel et al. (1996); (6):Hrivnak & Bieging (2005); (7):Fujii et al. (2001); (8):Klochkova & Chentsov (2007); (9):Sánchez Contreras et al. (2006); (10):Min et al. (2013); (11):Meixner et al. (2004); (12):Van Winckel & Reyniers (2000); (13):Gauba & Parthasarathy (2003); (14):Omont et al.

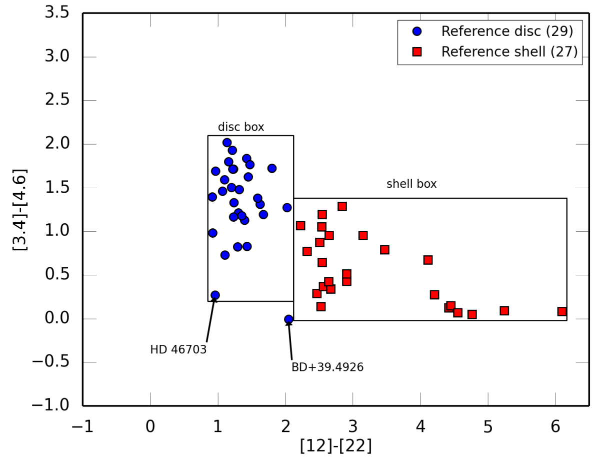

Figure 3. The WISE colour-colour diagram for the 56 reference sample is depicted here.

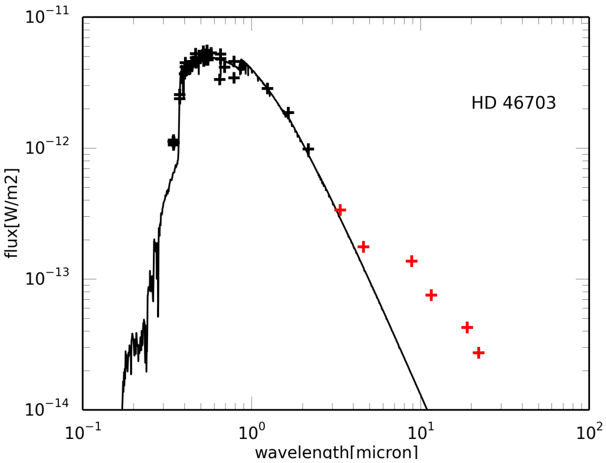

Figure 4. The SED of HD 46703. The symbols are the same as in Fig. 2

2.3 WISE colour-colour diagram of the reference sample

We display the WISE colour-colour diagram for our reference sample in Fig. 3. The 29 reference disc sources and 27 reference shell sources are represented with different symbols. The figure shows that our reference disc sources occupy a specific region in the WISE colour-colour diagram, which we define as the *disc box* (see Fig. 3). While determining the box, HD 46703 is included in the box, but BD+39°4926 is not. HD 46703 shows several excess points in its SED, and these are in various photometric systems (see Fig. 4). Its excess is thus reliably detected. In addition, it is a well studied, chemically peculiar binary object (Hrivnak et al. 2008). BD+39°4926, on the other hand, only exhibits a small excess at 22 μm, only detected in W4. We will discuss this source thoroughly in Sect. 5.

Reference shell sources occupy a larger area in the diagram. It is much harder to define them with a simple colour combination, because young shell sources may still have dust close enough to the stars as to show a [3.4]−[4.6] excess. For the evolved shells, the near-IR excess has disappeared, and they are expected to show only a red [12]−[22] colour. Consequently, we defined a big *shell box* which includes all reference shell sources.

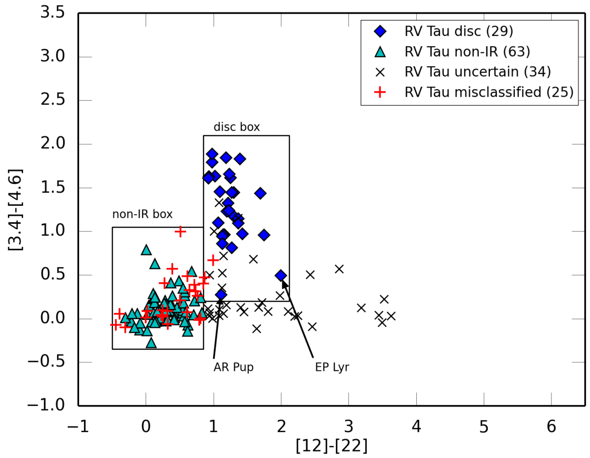

Figure 5. Three different type of SED characteristic among the Galactic RV Tauri stars and probably misclassified RV Tauri stars are represented here with different symbols.

3 RV TAURI STARS

We compare the infrared properties of RV Tauri stars with the reference sample in the WISE colour-colour diagram. In Fig. 5 we display the WISE colour-colour diagram for all 153 Galactic RV Tauri stars, which are given by the GCVS. However, 25 of the 153 RV Tauri stars are probably misclassified objects (Zsoldos 1991) because of their period range and spectral types. They are not included in our further analyses and we continue with 128 RV Tauri stars. Additionaly, for two well known RV Tauri stars, which are R Sct and V390 Vel, the WISE photometry suffers from saturation. These two objects are therefore are not included in the WISE colour-colour diagram either but are included in Table 2 for completeness.

RV Tauri stars cluster in three different regions in the WISE colour-colour diagram (see Fig. 5). In order to check this clustering we obtained full SEDs of all RV Tauri stars using the Vizier database as a source for the photometric data (Ochsenbein et al. 2000). For some of them, we used the appropriate scaled Kurucz model (Castelli & Kurucz 2003) with the stellar parameters taken from the literature (see the references in Table 2). For the sources where we lack indicative stellar parameters, we only analysed the reddened data. We note that the SEDs are affected by the large-amplitude pulsations.

The first striking clump is seen in the previously defined disc box. This box contains 38 RV Tauri, 29 of which show a clear disc SED. These are shown with diamonds in Fig.5. This clump is the WISE alternative of the RV Tauri box as defined by Lloyd Evans (1985). For the remaining 9 stars in the box, the full SED is not clear, which is likely due to the large amplitude of the pulsations in combination with a poor photometric sampling, which makes that the SED is not well defined. Several of these sources may actually have a disc excess, but pulsation and the poor wavelength

Table 2. A part of the RV Tau objects is given here. The full table is available online via CDS.

Name	RA	DEC	Spectral Type	[12]−[22]	[3.4]−[4.6]	SED	Ref
2MASS J05271262−6735074	05 27 12.62	−67 35 07.5		1.527	0.108	uncertain	
2MASS J11092679−6049285	11 09 26.793	−60 49 28.56		2.460	−0.089	uncertain	
2MASS J15183614+0204162	15 18 36.15	+02 04 16.3	F5	−0.131	0.058	non−IR excess	
2MASS J16571174−0403596	16 57 11.74	−04 03 59.7	F5	0.298	0.098	non−IR excess	
2MASS J19163578+3011388	19 16 35.78	+30 11 38.8	G0.2:e...	0.542	0.095	non−IR excess	
2MASS J21333241−0049057	21 33 32.41	−00 49 05.8	F9	1.450	0.079	uncertain	
AA Ari	02 03 37.73846	+22 52 22.2458	K7	0.125	0.185	non−IR excess	
AC Her	18 30 16.23850	+21 52 00.6080	F2Iep	1.271	1.448	disc	1
AD Aql	18 59 08.696	−08 10 14.12	G8	1.694	1.437	disc	1
AI Sco	17 56 18.5733	−33 48 43.359	G5	0.923	1.610	disc	1
⋮	⋮	⋮	⋮	⋮	⋮	⋮	⋮

(1):de Ruyter et al. (2006)

sampling makes their SEDs become unclear. Therefore, we classify these sources as *uncertain*.

Another remarkable clumping can be seen around the zero point of the diagram. These RV Tauri stars constitute a big part of the Galactic RV Tauri population. In total 63 RV Tauri stars occupy this region which we call the *non − IR box*.

Finally, some of the RV Tauri stars occupy the region which we defined as the shell box in the previous section. They show a mild [3.4]-[4.6] excess with 2.2 ⩽ [12]-[22] ⩽ 3.7, which indicates the presence of cool dust, characteristic of shell sources. However, they do not show a clear double-peaked SED as do the reference shell sources: in most cases only the [22] micron band is in excess. They could be potential shell sources but, due to the absence of information about envelope kinematics of these stars and the lack of more data in the IR to confirm the dusty excess, we prefer to classify them as *uncertain* sources.

After carefully examining the full SEDs we conclude that indeed all 29 (23%) RV Tauri stars which cluster in the disc box display a broad IR-excess in their SEDs. Many of them have already been given a disc status in the literature (de Ruyter et al. 2006; De Ruyter et al. 2005). The 63 (50%) RV Tauri stars, in the non-IR box do not display any IR excess at all, also not when considering their full SED. We called them as *non − IR* sources. Finally, 34 (27%) RV Tauri stars have an unclear SED and we label them as *uncertain* sources. The three groups are represented with different symbols in Fig. 5.

4 ANALYSIS

In our analyses we extensively used the literature to correlate SED characteristics with other observables. We focus on binarity as well as the presence of photospsheric chemical anomalies. We use the reference sample to investigate the Galactic RV Tauri population.

Table 3. Confirmed binaries among our whole sample. We give in the second column the SED types discussed in the main text.

Name	Type	P_{orbital}(day)	Ref
89 Her	pagb-disc	288.4	12
BD+39 4926	pagb	775.0	6
BD+46 442	pagb-disc	140.8	4
EN TrA	pagb-disc	1490.0	13
HD 108015	pagb-disc	938.0	5
HD 213985	pagb-disc	259.0	1
HD 44179	pagb-disc	298.0	9
HD 46703	pagb-disc	610.0	5
HD 52961	pagb-disc	1310.0	11
HD 95767	pagb-disc	2050.0	5
HR 4049	pagb-disc	429.0	9
IRAS05208−2035	pagb-disc	236.0	2
IRAS15469−5311	pagb-disc	389.9	13
IRAS17038−4815	pagb-disc	1381.0	1
IRAS19157−0247	pagb-disc	120.5	13
SAO 173329	pagb-disc	115.9	1
ST Pup	pagb-disc	410.0	3
AC Her	RVTauri-disc	1196.0	10
BD+03 3950	RVTauri-disc	519.6	13
IRAS09144−4933	RVTauri-disc	1770.0	1
RU Cen	RVTauri-disc	1489.0	1
SX Cen	RVTauri-disc	600.0	1
U Mon	RVTauri-disc	2597.0	8
V390 Vel	RVTauri-disc	499.0	7

(1):Gielen et al. (2008); (2):Gielen et al. (2011); (3):Gonzalez & Wallerstein (1996); (4):Gorlova et al. (2012); (5):Van Winckel et al. (2000); (6):Kodaira et al. (1970); (7):Maas et al. (2003); (8):Pollard & Cottrell (1995); (9):Van Winckel et al. (1995); (10):Van Winckel et al. (1998); (11):Waelkens et al. (1992); (12):Waters et al. (1993); (13):Van Winckel et al. (2009)

4.1 Disc and Binarity

There are 17 confirmed binaries among our reference sample. We indicated these 17 objects with blue circles in the WISE colour-colour diagram in Fig. 6. For the reference stars, the correlation between binarity and the presence of a disc SED is generally acknowledged (Van Winckel et al. 2009). Fig. 6 illustrates this statement most clearly, as the binary post-AGB objects are clearly clustered in the disc region of the diagram.

Direct detection of orbital motion in RV Tauri stars by means of radial velocity measurements is difficult because of the significant pulsational amplitude. Despite this difficulty, orbital elements have been determined for 7 RV Tauri stars so far. In Fig. 6 these binary RV Tauri stars are also represented, but with blue diamonds. The same binarity−disc SED correlation can also be seen for the RV Tauri stars. All confirmed binaries are listed in Table 3

RV Tauri photometric class b objects show a flux variation with a period much longer than their pulsation period. Van Winckel et al. (1999) has explained the RVb phenomenon by assuming that a circumbinary dusty disc is present and that the viewing angle onto the disc determines

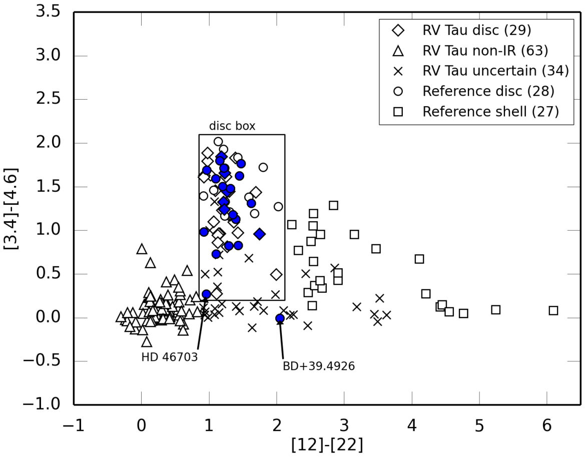

Figure 6. WISE [12]−[22], [3.4]−[4.6] colour-colour diagram of the merged reference+RV Tauri sample. Confirmed binares are shown in blue.

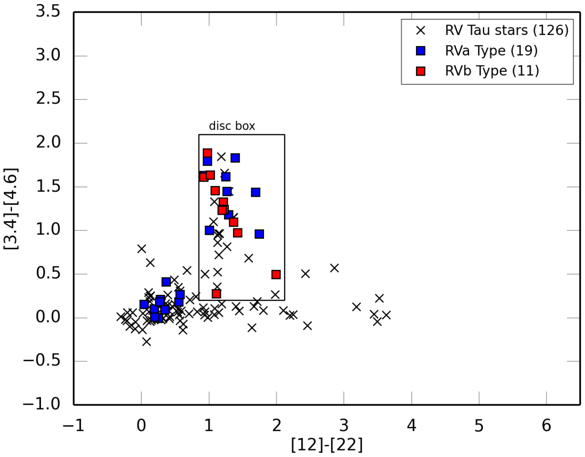

Figure 7. Photometric classification is represented with different colours in the WISE colour-colour diagram.

the photometric class. If the disc is seen under a high inclination, long-period variation may be seen due to variable circumstellar extinction during the orbital motion. Under this interpretation, the long-term period in the light curve is then the orbital period. If the system is seen with a small inclination (near pole-on), the line-of-sight is not obscured and no long-period variations will be detected. We have searched for RVa and RVb type classifications in the literature (Kiss et al. 2007; Rao & Giridhar 2014). We found 11 RVb and 20 RVa type objects. In Fig. 7 the RVa and RVb type RV Tauri stars are indicated with blue and red squares, respectively, in the WISE colour-colour diagram (R Sct is not included in the Fig. 7, since its WISE photometry suffers from saturation). All RVb stars are in the disc box and none are outside it. This corroborates the finding that the RVb phenomenon is related to the presence of circumstellar material. Discs with the correct inclination appear as RVb in the disc box. For 2 of 11 RVb objects (U Mon and SX Cen) and for 2 of 20 RVa objects (AC Her and RU Cen) the binary nature has been proven so far. An important difference between RVa and RVb type objects may very well be our viewing angle onto their circumstellar dust. More radial velocity monitoring is needed for all RVa and RVb objects to test their binary nature.

4.2 Disc and Chemical Depletion

In this study, one of our goals is to investigate whether there is a relation between infrared properties and the presence of the photospheric chemical anomaly called depletion. The most characteristic chemical signatures of depleted photospheres are high [Zn/Fe], [Zn/Ti] and [S/Ti] ratios. Waters et al. (1992) proposed that the most likely circumstance allowing the process occurs when the circumstellar dust is trapped in a circumstellar disc. Very strongly depleted atmospheres were first found exclusively in binary post-AGB objects (Van Winckel et al. 1995), but was found to be widespread in the last decennia.

As the [Zn/Ti] and [S/Ti] ratio's are good tracers for depleted photospheres, we used these abundance ratios, depending on their availability in the literature, as a tracer of depletion in our sources. We defined the objects as follows: if objects have [Zn/Ti] or [S/Ti] ratios larger than 1.5, they are classified as *strongly depleted*. If their [Zn/Ti] or [S/Ti] ratio is in the range 1.5−0.5, we classified them as *mildly depleted*. Finally, if objects have [Zn/Ti] or [S/Ti] ratio smaller than 0.5, we defined that there is no evidence for photospheric depletion and we labelled them as *not depleted*. The depletion quantifications are listed in the Table 5.

Waters et al. (1992) proposed that the most probable location for the depletion process to take place is in a dusty stable disc. For post-AGB stars, a stable disc is probably only present if the star resides in a binary system, as a orbiting disc can only be formed when the evolved star interacts closely with its companion. In a single post-AGB star, the mass loss in the AGB wind is expected to expand. Photospheric depletion patterns are observed in our reference post-AGB sample as in RV Tauri stars.

In Fig. 8 we present the depletion quantifications with different colours only for the reference sample. Strongly and mildly depleted objects are mostly concentrated in the disc region of the diagram. However, not all disc sources show depletion, as several disc objects are classified as not depleted. Moreover, there are 17 confirmed binary objects in the disc box of the WISE colour-colour diagram. All these binaries show a clear broad band SED (except BD+39°4926, which shows a small excess only in the WISE W4 band, see section 5) but for 4 of them there is no evidence for depletion. The only clear observable from Fig. 8 is that among the shell sources depletion is absent, so far and that the binarity is likely a necessary but not a sufficient requirement for depletion to occur.

In Fig. 9 we illustrate the depletion quantification for RV Tauri stars only. We show that RV Tauri stars follow the same trend as the reference post-AGB objects. Strongly and mildly depleted RV Tauri stars are mainly clustered in the disc box of the WISE colour-colour diagram. There are, however, also not-depleted objects in the disc box. One of these not-depleted objects is U Mon, which is a confirmed binary. Another interesting outlier is SS Gem. It is a strongly depleted object but it does not display a clear IR excess. All 7 RV Tauri stars whose orbital parameters have been measured so far show a clear disc SED, but not all of them

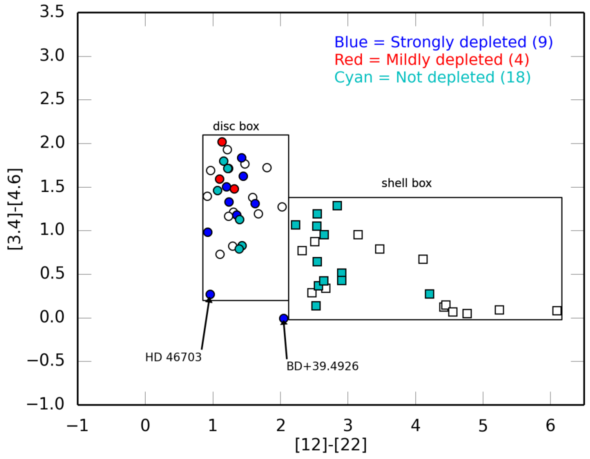

Figure 8. Depletion quantifications are shown with different colours for the reference sample.

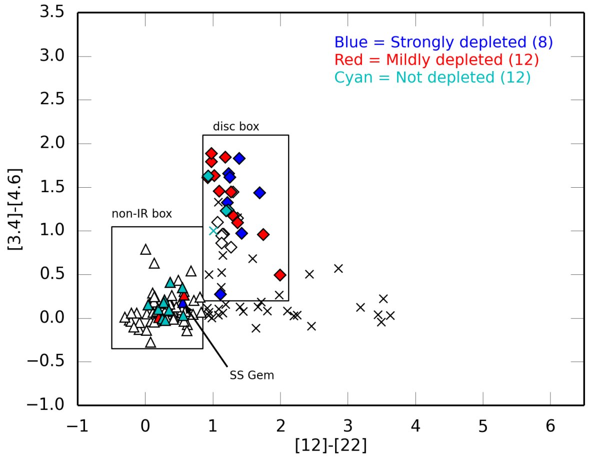

Figure 9. Depletion quantifications are shown with different colours for the Galactic RV Tauri stars.

are depleted and there are depleted objects without a dust excess.

Giridhar et al. (2005) have suggested that depletion is mostly observed in stars hotter than 5000 K. As the atmospheres of cooler stars have a deep convective envelope that mixes the accreted material with the whole convective part of the envelope and hence dilutes the effect of depletion. Venn et al. (2014) has also suggested the same scenario to explain not depleted RV Tauri stars with a disc. One can expect a lower depletion trend in function of effective temperature but it also depends on the mass ratio between the accreted material and the convective envelope. In Fig. 10 we illustrate effective temperature versus depletion quantification for the disc sources. We can see a general trend that hotter objects are, on general, somewhat more depleted, but there is clearly no strong relation between effective temperature and depletion.

Giridhar et al. (2005) has also suggested that depletion characteristics of RV Tauri stars may depend on their initial metallicity. Field RV Tauri classes of both spectroscopic classes A and B show depletion abundance patterns (see

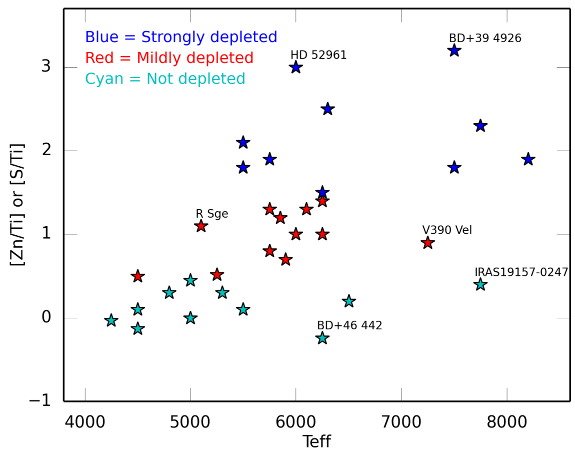

Figure 10. Effective temperature versus depletion quantifications is given here.

Table 4. Detailed information of the RV Tauri stars which are chemically studied up to now. $[F/H]_0$ gives the estimated initial metallicity obtained via the Zn or S abundance, PC gives the photometric class and SC gives the spectroscopic class of the RV Tauri sample star.

Name	$[F/H]_0$	PC	SC	$T_{\rm eff}$	Binarity	SED	Ref
Strongly depleted RV Tauri Stars.							
AD Aql	−0.10	a	B	6300		disc	2
AR Pup	0.40	b	B	6000		disc	5b,8
BD+03 3950	0.10	?	?	7750	Binary	disc	6
CT Ori	−0.60	a	B	5500		disc	5a,8
DY Ori	0.20	a	B	6000		disc	5b,7
IW Car	0.20	b	B	6700		disc	1,8
SS Gem	−0.20	a	A	5600		non−IR	5a
SX Cen	−0.30	b	B	6250	Binary	disc	6
Mildly depleted RV Tauri Stars.							
AC Her	−0.90	a	B	5900	Binary	disc	2
AZ Sgr		a	A	4750		non−IR	4,7
BT Lac	−0.10	b	A	5000		disc	7
EP Lyr	−0.90	b	B	6100		disc	5b,7
EQ Cas	−0.30	a	B	4500		non−IR	4
IRAS09144−4933	0.00	?	?	5750	Binary	disc	6
R Sge	0.10	b	A	5100		disc	5b
RU Cen	−1.10	a	B	6000	Binary	disc	6
RV Tau	−0.40	b	A	4500		disc	3
SU Gem	0.00	b	A	5250		disc	7
UY Ara	−0.30	a	B	5500		disc	3,7
V390 Vel	0.00	?	?	7250	Binary	disc	6
Not depleted RV Tauri Stars.							
AI Sco	−0.70	b	A	5300		disc	4,8
AR Sgr		a	A	5300		non−IR	4,7
BT Lib	−1.10	?	C	5800		non−IR	3
DF Cyg		a	A	4800		uncertain	4
DS Aqr		a	C	6500		non−IR	3
GP Cha	−0.60	b	A	5500		disc	6,7
R Sct	−0.20	a	A	4500		uncertain	3
RX Cap	−0.60	?	A	5800		non−IR	4
TT Oph	−0.80	a	A	4800		non−IR	3
TW Cam	−0.40	a	A	4800		disc	3
TX Oph	−1.10	?	A	5000		non−IR	4
U Mon	−0.50	b	A	5000	Binary	disc	3,8
UZ Oph	−0.80	a	A	5000		non−IR	4
V Vul	0.10	a	A	4500		disc	4,7
V360 Cyg	−1.30	a	C	5300		non−IR	2
V453 Oph	−2.20	a	C	5800		non−IR	2
V820 Cen	−2.20	a	C	4750		non−IR	7

(1):Giridhar et al. (1994); (2):Giridhar et al. (1998); (3):Giridhar et al. (2000); (4):Giridhar et al. (2005); (5a):Gonzalez et al. (1997b); (5b):Gonzalez et al. (1997a); (6):Maas et al. (2005); (7):Rao & Giridhar (2014); (8):Kiss et al. (2007)

Table 5). The initial metallicity, $[Fe/H]_0$, covered by these studies ranges from -0.1 to -0.8. The C-type RV Tauri stars in the field and in globular clusters do not show depletion patterns and their observed initial metallicities are smaller than -1.0. It may be indicating that the depletion process is not efficient at these low initial metallicities (Giridhar et al. 2000). The initial metallicity is, however, hard to determine in depleted objects. In Table 4 we list the chemically studied RV Tauri stars with their spectroscopic and photometric classes, effective temperature and initial metallicity. The C-type RV Tauri stars which are intrinsically metal poor objects are indeed not depleted while all the strongly depleted and mildly depleted objects are of spectroscopic class A or B. There are also many A-type objects which are not depleted.

5 DISCUSSION AND CONCLUSIONS

In this paper we compared RV Tauri stars with a reference sample of post-AGB objects concerning their infrared properties, binary nature and chemical abundances. Firstly, we showed that the RV Tauri stars are nicely clustered in the WISE colour-colour diagram and the clustering was confirmed by our detailed SED determinations. There are 128 RV Tauri variables in our Galaxy and 29 (23%) of them are disc sources, 63 (50%) of them are non-IR sources and 34 (27%) of them display an SED which we classify as uncertain. An example of each type of SED is presented in the Fig. 11. In this way, we stress that not all RV Tauri stars show an IR excess.

Secondly, we investigated the relation between infrared properties and binarity for both the RV Tauri stars and the reference post-AGB objects. Orbital parameters have been measured for 17 post-AGB objects and 7 RV Tauri stars. As all confirmed binaries are disc sources, we conclude that the correlation between the properties of the SED and binarity is obvious for both RV Tauri stars and post-AGB objects. As RV Tauri stars with a disc SED are suspected binaries, radial velocity monitoring experiments have been focussed on these systems so far. Indeed, all confirmed binary RV Tauri stars are disc sources. We conclude that binarity is a widespread phenomenon among the RV Tauri class of objects with discs but that only a minority of them have their orbital elements determined. Homogenous radial velocity measurements and CO observations are needed to come to general conclusions about the binary nature of RV Tauri stars as a whole.

Finally, we reviewed the chemical studies of both the RV Tauri stars and the reference post-AGB objects in the literature. We showed that for both groups the relation between infrared properties and chemical anomalies is complex. Strongly and mildly depleted objects are mostly disc sources but not exclusively so. 48% of the chemically studied reference post-AGB objects is depleted and they all display a clear broad band SED. The exception for the reference sample is BD+39°4926 which shows a small excess that has only been detected thanks to the sensitivity of the WISE experiment. Depletion is more widely observed in the RV Tauri stars. 56% of the chemically studied RV Tauri stars is depleted but not all of them are confirmed disc sources. Two of the depleted RV Tauri stars do not display a clear IR excess, but this seems to be exceptional. All the confirmed binaries are disc sources but not all of them are depleted. Thus, a disc is clearly not a sufficient condition for the dust-gas separation to take place but it does seem to be a prerequisite.

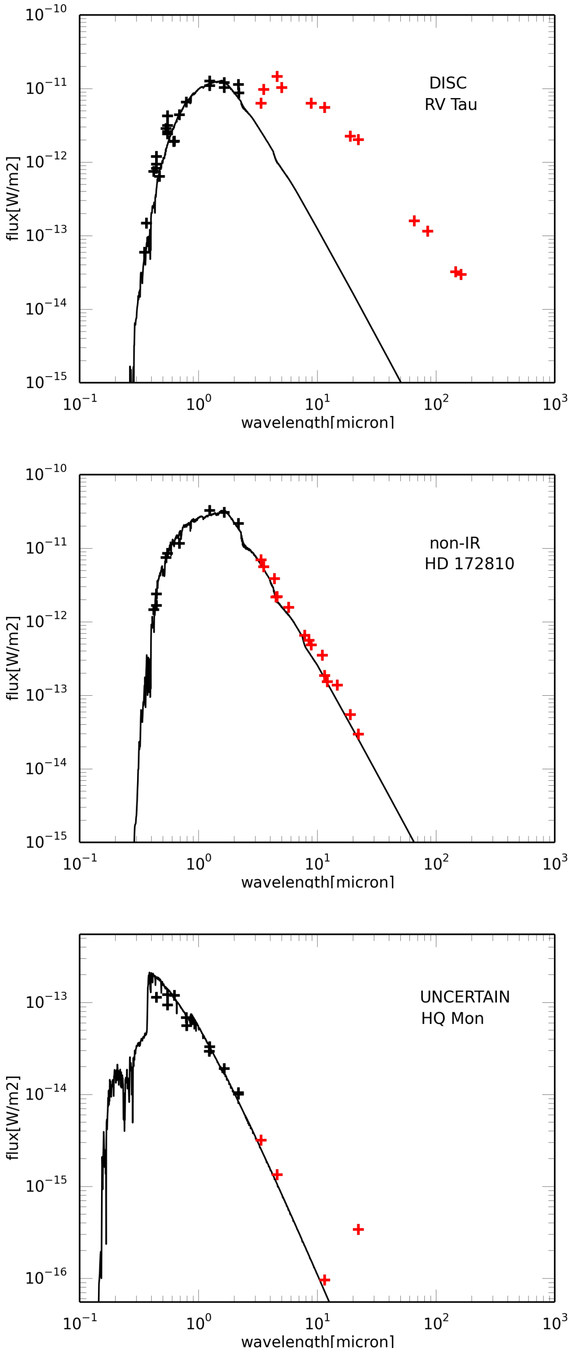

Figure 11. Prototypical SEDs of the three SED classes defined in this paper, in the RV Tauri case. Top panel: RV Tau, the prototype of the RV Tau class and a clear disc object. Middle panel: HD172810, an example of a non-IR excess source. Bottom panel: HQ Mon, one of the uncertain sources.

We conclude that (1) there are disc sources which do not show depletion patterns and the other way around (2) there are depleted sources without a dust excess. For the first case, the suggested scenario (Giridhar et al. 2005; Venn et al. 2014) is that a deep convective envelope may prevent the depletion signature to be observed. The main problem for

Table 5. Quantification of the depletion patterns obtained from the literature.

Name	Type	$[F/H]_0$	[Fe/H]	[Zn/Ti]	[S/Ti]	[Zn/Fe]	[C/Fe]	[s/Fe]	SED	Binarity	Ref
Strongly Depleted Objects.											
AD Aql	RV*	−0.10	−2.10	2.50	2.60	2.0	...	...	disc		2
AR Pup	RV*	0.40	−0.90				...	...	disc		5b
BD+03 3950	RV*	0.10	−0.30	2.30	2.60	0.4	...	...	disc	Binary	12
BD+39 4926	pA*	−0.10	−2.90		3.20		...	...	disc	Binary	10
CT Ori	RV*	−0.60	−1.90	1.90	2.00	1.3	...	...	disc		5a,22
DY Ori	RV*	0.20	−2.30	2.10	2.50	2.1	...	...	disc		5b
HD 213985	pA*		−0.90		1.90		...	...	disc	Binary	17
HD 44179	pA*	−0.60	−3.30			2.7	...	...	disc	Binary	17,18
HD 46703	sr*	−0.40	−1.60				...	...	disc	Binary	11
HD 52961	sr*		−4.80	3.00	3.35	3.4	...	...	disc	Binary	19
HR 4049	pA*	−0.40	−4.80			3.5	...	...	disc	Binary	17
IRAS15469−5311	OH*	0.20	0.00	1.80	2.10	0.3	...	...	disc	Binary	12
IRAS17038−4815	pA*		−1.50			0.3	...	...	disc	Binary	12
IRAS17233−4330	pA*	−0.20	−1.00	1.40	1.80	0.7	...	...	disc		12
IW Car	RV*	0.20	−1.00				...	...	disc		1
SS Gem	RV*	−0.20	−0.90	2.00	1.60	0.9	...	...	non−IR		5a
ST Pup	WV*	−0.10	−1.50	2.10	2.00	1.4	...	...	disc	Binary	6
SX Cen	RV*	−0.30	−1.10	1.50	1.90	0.6	...	...	disc	Binary	12
UY CMa	sr*	−0.40	−1.3	1.80	2.10	0.7	...	...	disc		4
Mildly Depleted Objects.											
AC Her	RV*	−0.90	−1.40	0.70	1.20	0.50	...	...	disc	Binary	2
AZ Sgr	RV*	−0.30	−1.60		1.30		...	...	non−IR		4
BT Lac	RV*	−0.10	−0.20	0.50		0.10	...	...	disc		15
EN Tra	Ce*		0.00	0.55	0.50	0.20	...	...	disc	Binary	20
EP Lyr	RV*	−0.90	−1.80	1.30	1.40	1.10	...	...	disc		5b
EQ Cas	RV*	−0.30	−0.80	1.00	1.00	0.50	...	...	non−IR		4
IRAS09144−4933	RV*	0.00	−0.30		1.30		...	...	disc	Binary	12
IRAS16230−3410	pA*	−0.40	−0.70	1.00	1.10	0.30	...	...	disc	Binary	12
LR Sco	sr*	0.20	0.00	0.80	0.60	0.20	...	...	disc		12
QY Sge	sr*	−0.20	−0.30	1.20	1.20	0.10	...	...	disc		12
R Sge	RV*	0.10	−0.50	1.10	1.70	0.30	...	...	disc		5b
RU Cen	RV*	−1.10	−1.90	1.00	1.30	0.90	...	...	disc	Binary	12
RV Tau	RV*	−0.40	−0.40	0.50		0.40	...	...	disc		3
SU Gem	RV*	0.00	−0.25	0.52	0.82	0.10	...	...	disc		15
UY Ara	RV*	−0.30	−1.00			0.70	...	...	disc		3
V390 Vel	RV*	0.00	−0.30	0.90	1.00	0.40	...	...	disc	Binary	12
Not Depleted Objects.											
AI Sco	RV*	−0.70		0.30	0.83	0.10	...	...	disc		4
AR Sgr	RV*		−1.33	0.01	0.39	0.10	...	...	non−IR		4
BD+46 442	*		−0.79	−0.24	−0.40	−0.08	...	...	disc	Binary	14
BT Lib	RV*	−1.10	−1.10			0.00	...	...	non−IR		3
DF Cyg	RV*		0.00	−0.74		−0.62	...	...	uncertain		4
DS Aqr	RV*		−1.10						non−IR		3
DY Aql	RV*		−1.00				...	...	non−IR		12
GP Cha	RV*	−0.60	−0.60	0.10	0.30	−0.10	...	...	disc		12
HD 108015	sr*		−0.09	0.10	0.11	−0.07	...	...	disc	Binary	20
IRAS06165+3158	IR*		−0.93	−0.03		−0.06	...	...	disc		15
IRAS09060−2807	sr*	−0.70	−0.70	0.20	0.00	0.10	...	...	disc		12
IRAS19157−0247	pA*	0.10	0.10		0.40		...	...	disc	Binary	12
R Sct	RV*	−0.20	−0.40	0.10		0.10	...	...	uncertain		3
RX Cap	RV*	−0.60	−0.80	0.00	0.00	0.20	...	...	non−IR		4
SAO 173329	Ir*		−0.92	−0.14	0.41	0.05	...	...	disc	Binary	21
TT Oph	RV*	−0.80	−0.80	0.00	0.80	0.00	...	...	non−IR		3
TW Cam	RV*	−0.40	−0.50	0.30	0.70	0.10	...	...	disc		3
TX Oph	RV*	−1.10	−1.2	0.00	0.56	−0.01	...	...	non−IR		4
U Mon	RV*	−0.50	−0.80	0.00	0.50	0.20	...	...	disc	Binary	3
UZ Oph	RV*	−0.80	−0.70	0.30	0.55	0.10	...	...	non−IR		4
V Vul	RV*	0.10	−0.40	−0.13	0.71	0.10	...	...	disc		4
V360 Cyg	RV*	−1.30	−1.40	−0.10	0.40	0.00	...	...	non−IR		2
V453 Oph	RV*	−2.20	−2.20	−0.03		0.40	...	...	non−IR		2
V820 Cen	RV*		−2.28	−0.07		0.40	...	...	non−IR		15
Not Depleted Objects (C and s−process Enhanced Objects).											
HD 187885	pA*	−0.60	...	...	...	...	1.00	1.10	shell		7
HD 235858	pA*	−0.82	...	...	...	...		1.99	shell		13
HD 56126	sr*	−1.00	...	...	...	...	1.10	1.50	shell		7
IRAS Z02229+6208	pA*	−0.50	...	...	...	...	0.80	1.40	shell		16
IRAS04296+3429	pA*	−0.60	...	...	...	...	0.80	1.50	shell		7
IRAS05113+1347	pA*	−0.75	...	...	...	...	1.09	2.00	shell		13
IRAS05341+0852	pA*	−0.80	...	...	...	...	1.00	2.20	shell		15
IRAS06530−0213	pA*	−0.90	...	...	...	...	1.30	1.90	shell		8
IRAS07430+1115	pA*	−0.50	...	...	...	...	0.60	1.60	shell		16
IRAS20000+3239	pA*	−1.40	...	...	...	...	1.70	1.40	shell		9
IRAS23304+6147	pA*	−0.81	...	...	...	...	0.91	1.60	shell		7
V448 Lac	sr*	−0.30					0.30	0.90	shell		7

(1):Giridhar et al. (1994); (2):Giridhar et al. (1998); (3):Giridhar et al. (2000); (4):Giridhar et al. (2005); (5a):Gonzalez et al. (1997b); (5b):Gonzalez et al. (1997a); (6):Gonzalez & Wallerstein (1996); (7):Van Winckel & Reyniers (2000); (8):Hrivnak & Reddy (2003); (9):Klochkova & Kipper (2006); (10):Kodaira et al. (1970); (11):Luck & Bond (1984); (12):Maas et al. (2005); (13):Reddy et al. (2002); (14):Gorlova et al. (2012) (15):Rao & Giridhar (2014); (16):Reddy et al. (1999); (17):Van Winckel et al. (1995); (18):Waelkens et al. (1996); (19):Waelkens et al. (1991); (20):Van Winckel (1997);(21):Rao et al. (2012);(22):Kiss et al. (2007)

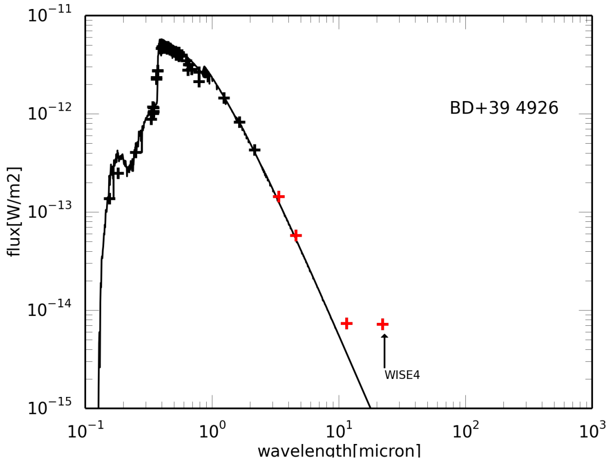

Figure 12. Spectral Energy Distribution of BD+39°4926.

this scenario is that it is unknown how strong the dilution is. For the latter case, the absence of a current infrared excess doesn't mean that such a disc was not present in a earlier evolutionary phase. The dust-gas separation operates on a certain timescale, thus, the dust reservoir may have already been exhausted while we can still detect the photospheric depletion pattern. The IR lifetime of a disc source will not only depend on the evolution of the central object, but it will also depend on the the evolution of the dusty disc itself.

Several detailed radiative transfer studies, some of which were constrained by high-spatial resolution interferometric observables, have shown that the dusty discs can be well modelled assuming as a passive, gas- and dust-rich irradiated disc (Dominik et al. 2003; Hillen et al. 2014). The evolution of these discs is not well documented yet and neither are the evolutionary processes themselves, nor the associated timescales. But the evolution of the disc will imply that the infrared position of these systems in the WISE colour-colour diagram will change accordingly.

The discs are subject to specific physical processes like grain growth, crystallisation (e.g. Gielen et al. 2011), and gas evaporation (Bujarrabal et al. 2013). It is likely that the infrared luminosity of the disc will gradually decline and will resemble the infrared properties of gas-poor debris discs. The depletion of the affected photospheres will, however, be visible much longer. The binary BD+39°4926 may represent such a case. The object has been long known to present chemical peculiarities (Kodaira et al. 1970). By now it is well characterised that this is due to a strong depletion of only the refractory elements. As noted also by (Venn et al. 2014) the detection of a small but significant IR excess is only recent and limited to the detection of an excess only in the WISE W4 band (Fig. 12). The binary motion and a first estimate of the orbital period were based on data with a poor radial velocity accuracy and a poor sampling (Kodaira et al. 1970). We therefore included this object in our long-term radial velocity monitoring programme (Van Winckel et al. 2010) using our HERMES spectrograph (Raskin et al. 2011). The orbital motion is clearly detected and in Fig. 13 we show the folded radial velocity data together with a fit representing the Keplerian solution. In Table 6 we present the full orbital elements of BD+39°4926 and the associated 1 σ uncertainties. These were obtained by a Monte-Carlo analyses in which we varied the original data point randomly within the specific uncertainty of the velocity points. As can be seen, also from Fig. 13, the orbital elements are very well determined. There is no observable to constrain the inclination. Using a 0.6 $M_\odot$ primary, the mass function of 0.381 $M_\odot$ translates into a minimal companion mass of 1 $M_\odot$ and a most probable one (assuming an inclination of 60°) of 1.3 $M_\odot$. We do not detect any flux contribution from the secondary, neither do we detect any symbiotic activity and we suspect that the companion is a non-evolved main sequence star.

Another good recently studied example of an evolved disc is AC Her (Hillen et al. 2015) whose interfermetric measurements show that the inner radius of the disc is large, the large grains have been settled to the midplane and the gas/dust ratio is small. Interestingly also BD+33°2642, the central star of the PN G052.7+50.7 was found to be a depleted (Napiwotzki et al. 1994) and recently found to be a binary as well (Van Winckel et al. 2014).

From these observables it seems that the depleted photospheres remain chemically peculiar for a longer time than the IR excess remains detectable. In the context of metal poor stars and the confusion between genuine metal poor stars (Venn et al. 2014) and strongly depleted stars, not only the presence of an infrared excess is important, but we show here that the binary nature of the object also seems to be a prerequisite for the depletion process to become active.

Our homogeneous infrared study of all Galactic RV Tauri stars shows that disc formation and hence likely binarity is indeed a widespread phenomenon (23%) but that also many RV Tauri stars exist which do not show an IR excess (50%) or show only an uncertain excess (27%).

The RV Tauri stars in the disc box share many observational properties of disc post-AGB stars and they are likely similar binary objects with the only difference that the RV Tauri stars happen to be in the population II Cepheid instability strip. The presence of a stable disc seems to be needed but not a sufficient condition for the depletion process to become efficient. More radial velocity monitoring is needed to investigate the binary properties of the whole disc sample.

The evolutionary status of the RV Tauri stars without an IR excess is less clear. As post-AGB stars with spectral types similar to these RV Tauri stars are expected to have a detectable IR-excess (Van Winckel 2003), the evolutionary nature of these objects remain to be clarified.

Many of the RV Tauri stars which are labelled *uncertain* have just one fluxpoint in excess which may indicate the presence of an expanding shell or evolved disc, but more IR data is needed to test this. If confirmed expanding shells, then these objects may be similar in evolutionary nature to the shell sources among the post-AGB reference sample. If confirmed evolved discs then these objects should be binaries in a more evolved evolutionary stages as the disc objects.

In our following paper we will deal with a systematic abundance analysis of RV Tauri stars covering all three different SED types: disc SEDs, uncertain SEDs and SEDs without a dust excess. We will futher investigate the impact of a disc onto the chemical diversity and study the evolutionary picture of RV Tauri stars via systematic studies of their photospheric composition.

Table 6. Orbital elements of BD+39°4926

Parameter	Value	σ
P (d)	873.06	0.64
$a\ sini$ (AU)	1.296	0.004
$f(m)$ ($M_\odot$)	0.381	0.004
K (km/s)	16.16	0.05
e	0.032	0.003
ω (°)	105	3
T_0 (JD)	2 455 420.	18
γ (km/s)	-30.66	0.03
varreduc	99.85	

Note. Orbital parameters with their uncertainties and the variance reduction of the orbital fit expressed in percentage of the original variance of the raw radial velocity data.

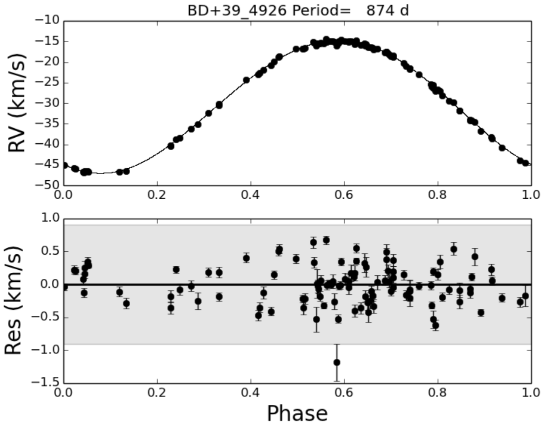

Figure 13. The radial velocity curve of BD+39°4926.

ACKNOWLEDGMENTS

The authors dedicate this paper to Tom Lloyd Evans (1940−2014).

This work has been performed thanks to 2214-A International Research Fellowship Programme of the Scientific and Technological Research Council of Turkey (TUBITAK).

IG would like to thank KU Leuven Astronomy Institute for their kind hospitality.

Based on observations made with the Mercator Telescope, operated on the island of La Palma by the Flemish Community, at the Spanish Observatorio del Roque de los Muchachos of the Instituto de Astrofsica de Canarias.

Based on observations obtained with the HERMES spectrograph, which is supported by the Fund for Scientific Research of Flanders (FWO), Belgium, the Research Council of K.U.Leuven, Belgium, the Fonds National de la Recherche Scientifique (F.R.S.-FNRS), Belgium, the Royal Observatory of Belgium, the Observatoire de Genve, Switzerland and the Thringer Landessternwarte Tautenburg, Germany.

HVW, MH, RM, DK acknlowledge support of the KU Leuven contract GOA/13/012. DK acknowledges support of the FWO grant G.OB86.13.

The following Internet-based resources were used in research for this paper: the NASA Astrophysics Data System; the SIMBAD database and the VizieR service operated by CDS, Strasbourg, France.

REFERENCES

Alcock C., Allsman R. A., Alves D. R., et al. 1998, AJ, 115, 1921

Buchler J. R., Wood P. R., Soszyński I., 2009, ApJ, 698, 944

Bujarrabal V., 1999, in Le Bertre T., Lebre A., Waelkens C., eds, Asymptotic Giant Branch Stars Vol. 191 of IAU Symposium, AGB circumstellar envelopes: molecular observations. p. 363

Bujarrabal V., Alcolea J., Van Winckel H., Santander-García M., Castro-Carrizo A., 2013, A&A, 557, A104

Bujarrabal V., Castro-Carrizo A., Alcolea J., Sánchez Contreras C., 2001, A&A, 377, 868

Bujarrabal V., Castro-Carrizo A., Alcolea J., Van Winckel H., 2015, A&A, 575, L7

Bujarrabal V., Castro-Carrizo A., Alcolea J., Van Winckel H., Sánchez Contreras C., Santander-García M., Neri R., Lucas R., 2013, A&A, 557, L11

Castelli F., Kurucz R. L., 2003, in Piskunov N., Weiss W. W., Gray D. F., eds, Modelling of Stellar Atmospheres Vol. 210 of IAU Symposium, New Grids of ATLAS9 Model Atmospheres. p. 20P

De Ruyter S., Van Winckel H., Dominik C., Waters L. B. F. M., Dejonghe H., 2005, A&A, 435, 161

de Ruyter S., van Winckel H., Maas T., Lloyd Evans T., Waters L. B. F. M., Dejonghe H., 2006, A&A, 448, 641

Degroote P., Acke B., Samadi R., Aerts C., Kurtz D. W., Noels A., Miglio A., Montalbán J., Bloemen S., Baglin A., Baudin F., Catala C., Michel E., Auvergne M., 2011, A&A, 536, A82

Deroo P., Acke B., Verhoelst T., Dominik C., Tatulli E., Van Winckel H., 2007, A&A, 474, L45

Deroo P., Reyniers M., Van Winckel H., Goriely S., Siess L., 2005, A&A, 438, 987

Deroo P., van Winckel H., Min M., Waters L. B. F. M., Verhoelst T., Jaffe W., Morel S., Paresce F., Richichi A., Stee P., Wittkowski M., 2006, A&A, 450, 181

Dominik C., Dullemond C. P., Cami J., van Winckel H., 2003, A&A, 397, 595

Fokin A. B., 1994, A&A, 292, 133

Fujii T., Nakada Y., Parthasarathy M., 2001, in Szczerba R., Górny S. K., eds, Astrophysics and Space Science Library Vol. 265 of Astrophysics and Space Science Library, BVRIJHK Photometry of Post-AGB Candidates: Evolution of Post-AGB Central Stars. p. 45

Gauba G., Parthasarathy M., 2003, A&A, 407, 1007

Gehrz R. D., 1972, ApJ, 178, 715

Gehrz R. D., Ney E. P., 1972, Publ. Astron. Soc. Pac., 84, 768

Gehrz R. D., Woolf N. J., 1970, ApJ, 161, L213

Gielen C., Bouwman J., van Winckel H., Lloyd Evans T., Woods P. M., Kemper F., Marengo M., Meixner M., Sloan G. C., Tielens A. G. G. M., 2011, A&A, 533, A99

Gielen C., van Winckel H., Min M., Waters L. B. F. M., Lloyd Evans T., 2008, A&A, 490, 725

Gielen C., Van Winckel H., Reyniers M., Zijlstra A., Lloyd Evans T., Gordon K. D., Kemper F., Indebetouw R., Marengo M., Matsuura M., Meixner M., Sloan G. C., Tielens A. G. G. M., Woods P. M., 2009, A&A, 508, 1391

Gielen C., van Winckel H., Waters L. B. F. M., Min M., Dominik C., 2007, A&A, 475, 629

Giridhar S., Lambert D. L., Gonzalez G., 1998, ApJ, 509, 366

Giridhar S., Lambert D. L., Gonzalez G., 2000, ApJ, 531, 521

Giridhar S., Lambert D. L., Reddy B. E., Gonzalez G., Yong D., 2005, ApJ, 627, 432

Giridhar S., Rao N. K., Lambert D. L., 1994, ApJ, 437, 476

Gonzalez G., Lambert D. L., Giridhar S., 1997a, ApJ, 481, 452

Gonzalez G., Lambert D. L., Giridhar S., 1997b, ApJ, 479, 427

Gonzalez G., Wallerstein G., 1996, MNRAS, 280, 515

Gorlova N., Van Winckel H., Gielen C., Raskin G., Prins S., Pessemier W., Waelkens C., Frémat Y., Hensberge H., Dumortier L., Jorissen A., Van Eck S., 2012, A&A, 542, A27

He J. H., Szczerba R., Hasegawa T. I., Schmidt M. R., 2014, ApJS, 210, 26

Herwig F., 2005, ARA&A, 43, 435

Hillen M., de Vries B. L., Menu J., Van Winckel H., Min M., Mulders G. D., 2015, A&A, 578, A40

Hillen M., Menu J., Van Winckel H., Min M., Gielen C., Wevers T., Mulders G. D., Regibo S., Verhoelst T., 2014, A&A, 568, A12

Hillen M., Verhoelst T., Van Winckel H., Chesneau O., Hummel C. A., Monnier J. D., Farrington C., Tycner C., Mourard D., ten Brummelaar T., Banerjee D. P. K., Zavala R. T., 2013, A&A, 559, A111

Hrivnak B. J., Bieging J. H., 2005, ApJ, 624, 331

Hrivnak B. J., Lu W., Bohlender D., Morris S. C., Woodsworth A. W., Scarfe C. D., 2011, ApJ, 734, 25

Hrivnak B. J., Reddy B. E., 2003, ApJ, 590, 1049

Hrivnak B. J., Van Winckel H., Reyniers M., Bohlender D., Waelkens C., Lu W., 2008, AJ, 136, 1557

Hrivnak B. J., Volk K., Kwok S., 2000, ApJ, 535, 275

Jura M., 1986, ApJ, 309, 732

Kiss L. L., Derekas A., Szabó G. M., Bedding T. R., Szabados L., 2007, MNRAS, 375, 1338

Klochkova V. G., Chentsov Y. L., 2007, Astronomy Reports, 51, 994

Klochkova V. G., Kipper T., 2006, Baltic Astronomy, 15, 395

Kodaira K., Greenstein J. L., Oke J. B., 1970, ApJ, 159, 485+

Kukarkin B. V., 1958, in Roman N. G., ed., Comparison of the Large-Scale Structure of the Galactic System with that of Other Stellar Systems Vol. 5 of IAU Symposium, Variable stars and problems of general structure of galaxies. p. 49

Lloyd Evans T., 1985, MNRAS, 217, 493

Lloyd Evans T., 1999, in IAU Symp. 191: Asymptotic Giant Branch Stars Vol. 191, The nature of rv tauri stars. p. 453

Luck R. E., Bond H. E., 1984, ApJ, 279, 729

Maas T., Giridhar S., Lambert D. L., 2007, ApJ, 666, 378

Maas T., Van Winckel H., Lloyd Evans T., 2005, A&A, 429, 297

Maas T., Van Winckel H., Lloyd Evans T., Nyman L.-Å., Kilkenny D., Martinez P., Marang F., van Wyk F., 2003, A&A, 405, 271

Maas T., Van Winckel H., Waelkens C., 2002, A&A, 386, 504

Meixner M., Zalucha A., Ueta T., Fong D., Justtanont K., 2004, ApJ, 614, 371

Min M., Jeffers S. V., Canovas H., Rodenhuis M., Keller C. U., Waters L. B. F. M., 2013, A&A, 554, A15

Molster F. J., Waters L. B. F. M., Tielens A. G. G. M., 2002, A&A, 382, 222

Molster F. J., Waters L. B. F. M., Tielens A. G. G. M., Barlow M. J., 2002, A&A, 382, 184

Molster F. J., Waters L. B. F. M., Tielens A. G. G. M., Koike C., Chihara H., 2002, A&A, 382, 241

Napiwotzki R., Heber U., Koeppen J., 1994, A&A, 292, 239

Ochsenbein F., Bauer P., Marcout J., 2000, A&A, 143, 23

Omont A., Loup C., Forveille T., te Lintel Hekkert P., Habing H., Sivagnanam P., 1993, A&A, 267, 515

Oudmaijer R. D., Waters L. B. F. M., van der Veen W. E. C. J., Geballe T. R., 1995, A&A, 299, 69

Pollard K. H., Cottrell P. L., 1995, in ASP Conf. Ser. 83: IAU Colloq. 155: Astrophysical Applications of Stellar Pulsation The Long-term Variation in the RV Tauri Star U MON. pp 409–+

Pollard K. R., Cottrell P. L., Lawson W. A., Albrow M. D., Tobin W., 1997, MNRAS, 286, 1

Preston G. W., Krzeminski W., Smak J., Williams J. A., 1963, ApJ, 137, 401

Rao S. S., Giridhar S., 2014, Rev. Mex. Fis., 50, 49

Rao S. S., Giridhar S., Lambert D. L., 2012, MNRAS, 419, 1254

Raskin G., van Winckel H., Hensberge H., et al. 2011, A&A, 526, A69

Reddy B. E., Bakker E. J., Hrivnak B. J., 1999, ApJ, 524, 831

Reddy B. E., Lambert D. L., Gonzalez G., Yong D., 2002, ApJ, 564, 482

Reyniers M., Abia C., Van Winckel H., Lloyd Evans T., Decin L., Eriksson K., Pollard K. R., 2007, A&A, 461, 641

Reyniers M., Van Winckel H., 2007, A&A, 463, L1

Samus N. N., Durlevich O. V., et al. 2009, VizieR Online Data Catalog, 1, 2025

Sánchez Contreras C., Bujarrabal V., Castro-Carrizo A., Alcolea J., Sargent A., 2006, ApJ, 643, 945

Soszyñski I., Udalski A., Szymañski M. K., Kubiak M., Pietrzyñski G., Wyrzykowski Ł., Ulaczyk K., Poleski R., 2010, Acta Astron., 60, 91

Soszyński I., Udalski A., Szymański M. K., Kubiak M., Pietrzyński G., Wyrzykowski Ł., Szewczyk O., Ulaczyk K., Poleski R., 2008, Acta Astron., 58, 293

Tuchman Y., Lebre A., Mennessier M. O., Yarri A., 1993, A&A, 271, 501

Van Winckel H., 1997, A&A, 319, 561

Van Winckel H., 2003, ARA&A, 41, 391

Van Winckel H., Jorissen A., Exter K., Raskin G., Prins S., Perez Padilla J., Merges F., Pessemier W., 2014, A&A, 563, L10

Van Winckel H., Jorissen A., Gorlova N., Dermine T., Exter K., Masseron T., Østensen R., Van Eck S., Van de Steene G., 2010, MemSAI, 81, 1022

Van Winckel H., Lloyd Evans T., Briquet M., et al. 2009, A&A, 505, 1221

Van Winckel H., Oudmaijer R. D., Trams N. R., 1996, A&A, 312, 553

Van Winckel H., Reyniers M., 2000, A&A, 354, 135

Van Winckel H., Waelkens C., Fernie J. D., Waters

L. B. F. M., 1999, A&A, 343, 202

Van Winckel H., Waelkens C., Waters L. B. F. M., 1995, A&A, 293, L25

Van Winckel H., Waelkens C., Waters L. B. F. M., 2000, in IAU Symposium Vol. 177, Binary "Post-AGB" Stars. pp 285–+

Van Winckel H., Waelkens C., Waters L. B. F. M., Molster F. J., Udry S., Bakker E. J., 1998, A&A, 336, L17

Venn K. A., Puzia T. H., Divell M., Côté S., Lambert D. L., Starkenburg E., 2014, ApJ, 791, 98

Waelkens C., Van Winckel H., Bogaert E., Trams N. R., 1991, A&A, 251, 495

Waelkens C., Van Winckel H., Trams N. R., Waters L. B. F. M., 1992, A&A, 256, L15

Waelkens C., Van Winckel H., Waters L. B. F. M., Bakker E. J., 1996, A&A, 314, L17

Wannier P. G., Sahai R., Andersson B.-G., Johnson H. R., 1990, ApJ, 358, 251

Waters L. B. F. M., Trams N. R., Waelkens C., 1992, A&A, 262, L37

Waters L. B. F. M., Waelkens C., Mayor M., Trams N. R., 1993, A&A, 269, 242

Woods P. M., Nyman L.-Å., Schöier F. L., Zijlstra A. A., Millar T. J., Olofsson H., 2005, A&A, 429, 977

Wright E. L., Eisenhardt P. R. M., Mainzer A. K., et al. 2010, AJ, 140, 1868

Zsoldos E., 1991, Information Bulletin on Variable Stars, 3557, 1